Co-location of the downdip end of seismic locking and the continental shelf break

Luca C. Malatesta[1,2,*], Lucile Bruhat[3], Noah J. Finnegan[1]

[1]Department of Earth and Planetary Sciences, University of California Santa Cruz, Santa Cruz, California, USA.
[2]Institute of Earth Surface Dynamics, University of Lausanne, Lausanne, Switzerland.
[3]Department of Geology, École Normale Supérieure, Paris, France
*corresponding author: luca.malatesta@unil.ch

Abstract

In subduction zones, onshore geodesy provides the main data used to map seismic locking on the plate interface. We propose a new offshore control by establishing the co-location of the shelf break and the locking depth based on the Cascadia subduction. The erosive shelf of a subduction margin results from continuous uplift and active wave erosion. The long-term uplift is driven by 1) the non-recoverable fraction of interseismic deformation and 2) continental uplift (e.g. isostasy). We combine a wave erosion model with an elastic deformation model to show how the hinge line that marks the transition from interseismic subsidence to uplift pins the location of the shelf break. A global compilation of subduction zones with well resolved locking depths confirms our model with shelf breaks lying much closer to the locking depth than coastlines. Subduction margin morphology integrates hundreds of seismic cycles and informs seismic coupling stability through time.

Introduction

The portion of a subduction zone plate interface that is frictionally locked between earthquakes controls the size of megathrust ruptures (Aki, 1967; Mai and Beroza, 2000). Strain accumulation from locking on the plate interface produces interseismic deformation at the surface, which can be inverted to determine the extent of the locked region on the fault, following the widely used back-slip model (Savage, 1983). This procedure has been used for decades to produce maps of locking, also referred to as coupling, over subduction zones (e.g. Yoshioka et al., 1993; Sagiya, 1999; Mazzotti et al., 2000; Nishimura et al., 2004; Simoes et al., 2004; Chlieh et al., 2008; Metois et al., 2012). However, due to the short duration of geodetic measurements, these inversions typically reflect a fraction of the earthquake cycle, which could be contaminated by transient slip events (Dragert et al., 2001; Obara, 2002), or deformation unrelated to the megathrust (e.g. postglacial rebound, James et al., 2009). Because the locked region is typically offshore, it may also be poorly constrained simply due to the concentration of geodetic measurements on shore. This problem is compounded by wide continental shelves (Wang and Tréhu, 2016). Seafloor geodesy can overcome some of these problems, but remains uncommon (Bürgmann and Chadwell, 2014).

On land, tectonic geomorphology complements short duration geodetic and seismic records and provides a geologically more meaningful tectonic record (e.g. Valensise and Ward, 1991; Lavé and Avouac, 2001; Brooks et al., 2011). During the seismic cycle, crustal deformation is considered as almost entirely elastic, but over geological timescale, herein *long-term*, it is the anelastic fraction that builds mountains (Avouac, 2003).

Although little work has linked submarine geomorphology and subduction zone deformation, Ruff and Tichelaar (1996) identified a correlation between the downdip end of subduction zone rupture and the position of the coastline. This correlation fits the Andean subduction particularly well, and Saillard et al. (2017) suggested that the distribution of anelastic interseismic deformation could explain it. The coastline, however, is modified primarily by fluctuations in sea level and erosion and deposition, not tectonics.

Since the compilation by Ruff and Tichelaar (1996), advances in geodetic inversions for interseismic coupling allows renewed scrutiny of potential relationships between subduction zone locking and coastal morphology. Towards this end, we develop here a model of wave erosion across a subduction margin where long-term vertical deformation is driven by the anelastic fraction of the interseismic deformation. Our results show that an erosive continental shelf (gentle platform at less than 200 m below modern sea level) forms as a natural consequence of uplift and wave erosion along an active margin. The outer edge of this shelf is anchored by the location of the downdip end of seismic coupling on the megathrust (i.e. the locking depth). We first test this coupled model on the morphology of the Cascadia subduction zone. Then, a global examination of data from seven active subduction zones where locking depths are well constrained reveals that the edge of the continental shelf is a much better predictor of the locking depth than is the coastline. We conclude that the morphology of the continental shelf constrains the extent of the locked region integrated over many earthquake cycles in subduction zones.

Relationship between coastal morphology and interseismic coupling

The Cascadia shelf break is co-located with the downdip end

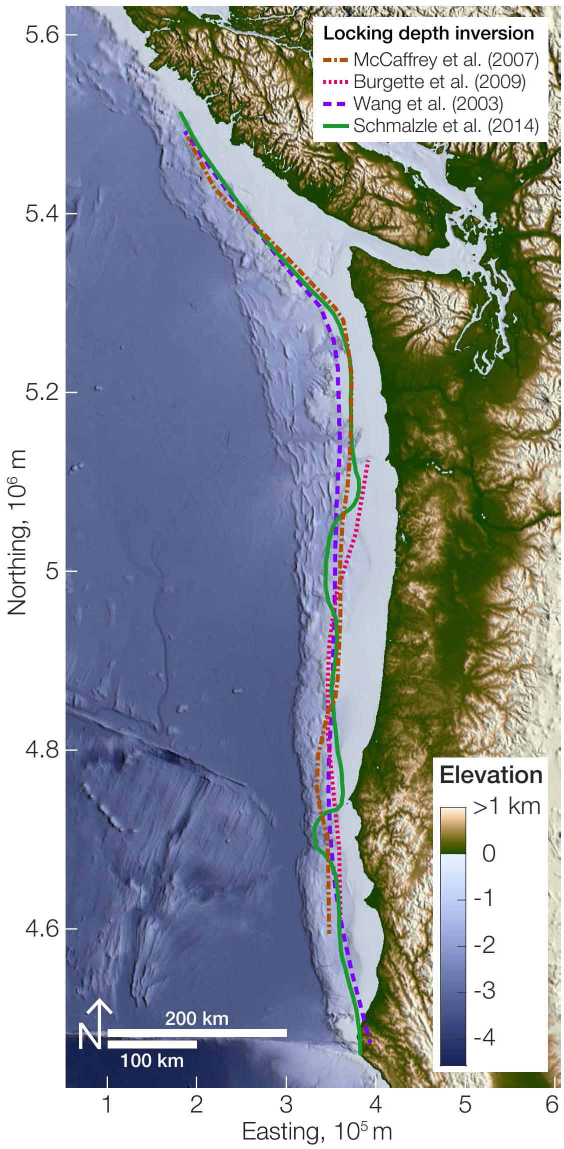

Figure 1: Solutions for the downdip end of seismic coupling in Cascadia, derived from GPS (Wang et al., 2003; McCaffrey et al., 2007; Schmalzle et al., 2014) and road leveling (Burgette et al., 2009), follow the edge of the continental shelf and are removed from the coastline. The locking depth is outlined for a value of ∼80% locking. Color map from Crameri (2018).

of coupling.

The Cascadia subduction zone does not appear in Ruff and Tichelaar (1996), as the compilation was published before precise geodesy. Nonetheless, geological evidence of M8-9 earthquakes have since revealed Cascadia's substantial seismic hazard (Satake et al., 1996, 2003). When evaluating seismic hazard subduction zones, the determination of the locking depth remains critical because a deeper rupture implies larger coseismic slip close to coastal regions. Most inversions for slip rates of geodetic measurements set the megathrust to be fully locked to a depth of 10–20 km (Hyndman and Wang, 1995; Wang et al., 2003; Burgette et al., 2009; McCaffrey et al., 2013; Schmalzle et al., 2014; Krogstad et al., 2016; Bruhat and Segall, 2016).

Figure 1 displays examples of solutions for the position of the locking depth inverted from GPS, tide gauges measurements, and road leveling surveys. They all show a striking divergence from the locking depth-coast relationship proposed by Ruff and Tichelaar (1996). Instead, along the Cascadia margin and its wide shelf (∼60 km), the locking depth appears to closely co-locate with the shelf-break, not the coastline. Indeed, Goldfinger et al. (1992) and McNeill et al. (2000) noted that the outer arc high — the edge of the shelf in Cascadia — conspicuously follows the location of the locking depth.

The morphology of compressional active margins is primarily controlled by subsidence, thrusting and sedimentation on the continental slope (Fuller et al., 2006; Cubas et al., 2013), and by the competition between uplift and erosion in the shallow marine to create and maintain an erosive shelf (Bradley and Griggs, 1976; Anderson et al., 1999). Consequently, the hinge line that marks the transition from offshore subsidence to landward continental uplift is of primary importance in anchoring the continental shelf edge. We propose that this hinge-line is localized approximately above the locking depth (Savage, 1983) by the pattern of interseismic deformation (Figure 2 top) that results from the extent of the locked and transitional domains of the megathrust (Figure 2 bottom).

Spatial distribution of long-term uplift

Numerical models of coastal landscape evolution commonly use spatially uniform uplift (Anderson et al., 1999; Snyder et al., 2002; Melnick, 2016), we hypothesize that long-term vertical deformation derives from a non-uniform interseismic loading. At the end of an earthquake cycle, a fraction of the interseismic deformation is not recovered. This anelastic deformation should roughly follow the same spatial distribution as the elastic deformation.

Although it has never been fully physically demonstrated, the relationship between long-term deformation and interseismic elastic patterns has been frequently observed. Allmendinger et al. (2009) noted that "at a regional scale within continents, interseismic deformation is mostly nearly similar to regional late Cenozoic tectonic deformation". Work from Loveless and Allmendiger (2005) showed that the extensional strain field predicted by elastic interseismic deformation co-locates with regions of normal faulting in the Coastal Cordillera of Chile. Stevens and Avouac (2015) noted that the uplift pattern predicted by their coupling inferred from geodesy above the Main Himalayan Thrust mimics the topography above the thrust. Coastal uplift above subduction zones has also been attributed to interseismic deformation based on the pattern of deformed terraces in Cascadia (Kelsey and Bockheim, 1994; Personius, 1995), on the co-location of peninsulas and shallow locking depth in the Andes (Saillard et al., 2017), and on the growth of the Japanese coastal mountains (Yoshikawa, 1968; Yoshikawa et al., 1981; Le Pichon et al., 1998). From the numerical modeling side, when looking at uplift predicted by elasto-visco-plastic models for crustal deformation, Cattin and Avouac (2000) and Vergne et al. (2001) demonstrated that permanent vertical deformation mimics the elastic interseismic deformation. The seismic cycle analogue model by Rosenau et al. (2009) shows permanent interseismic uplift at the coastline.

The traditional back-slip approach assumes that all deformation occurs elastically on the plate interface and therefore does not produce vertical long-term deformation. However, once we consider that interseismic deformation is not limited to a contact plane, but affects two plates of non-negligible thicknesses, the amplitude of the elastic interseismic field changes. Kanda and Simons (2010) showed in fact that, compared to the back-slip model, vertical interseismic rates are enhanced for thicker plates, due to plate bending, and roughly follow the same spatial distribution. In that context, our study would assume that, when the megathrust slips, deformation mostly localizes on the plate interface and the elastic deformation predicted by the back-slip method is recovered, while the extra deformation caused by flexural effects is not. It seems then reasonable to consider that, at the end of the earthquake cycle, the net deformation distribution would follow the original interseismic profile.

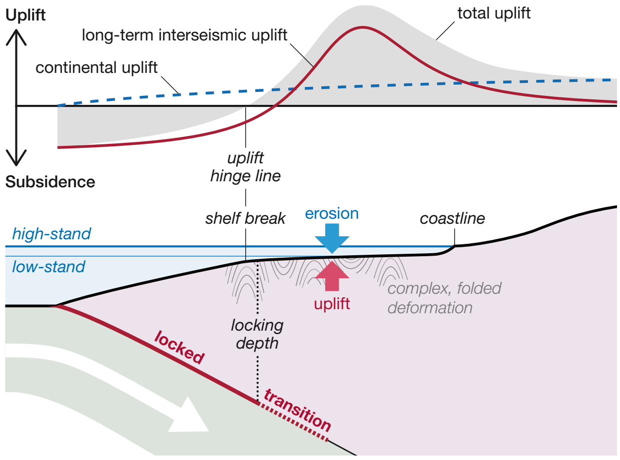

Figure 2: An erosive continental shelf requires wave-base erosion and rock uplift. These conditions are met landward of the uplift hinge line set by the combined patterns of interseismic and continental uplift (top). The shelf break is anchored at the hinge line, and the shelf can grow landward by coastal retreat (bottom). The interseismic deformation is controlled by the pattern of locked, transitional, and creeping segments of the megathrust.

Model coupling wave erosion and interseismic uplift explains Cascadia

We explore submarine topographic expression of long-term interseismic locking on a subduction megathrust as follows (Figure 3). For marine erosion, we adopt the model of Anderson et al. (1999) that expends ocean wave energy on the shallow seafloor for wave-base erosion, leaving the remainder for sea-cliff erosion. The erosion component is driven by the sea level curve of Spratt and Lisiecki (2016) looped over 2 Myr for a naturally noisy and high-resolution eustatic signal. Wave energy is assumed constant through time. Marine erosion is coupled to long-term tectonic uplift derived from the interseismic field and a secular continental uplift component. Spatial distribution of long-term uplift rates is computed with a back-slip model (Savage, 1983) using half-space elastic Green's functions (Okada, 1992) assuming a fully locked region above the locking depth (see Bruhat and Segall, 2016, for details). The back-slip model assumes that surface deformation is due to elastic strain accumulation on the plate interface and that it is equivalent to normal slip in the locked region. We compute the distribution of interseismic surface uplift rates at an elevation of 0 m. Following estimates by Le Pichon et al. (1998) and van Dinther et al. (2013), we use a fraction (5%) of that deformation profile as long-term field of uplift (Figure 3A). The uplift hinge line predicted by the back-slip model is generally located within 5 km of the locking depth but can be displaced seaward in the absence of a transitional zone of partial locking and a gently dipping ($< 10°$) slab (supplementary Figure S1). The other uplift component is a generalized term for all components of continental uplift, including isostatic response to denudation, underplating, and intracontinental compressional tectonics. It is modeled as an exponentially decaying uplift rate reaching zero at the trench (Figure 3A). If the continental uplift is much larger than the interseismic uplift, the hinge line of total uplift is displaced seaward (Figure 3C).

The numerical model presented

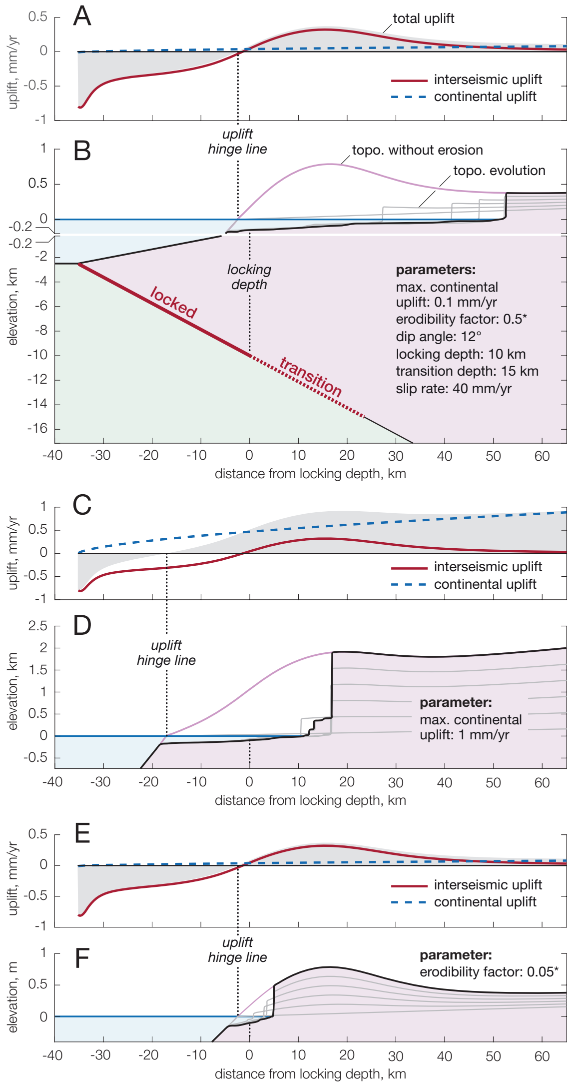

Figure 3: The numerical model is forced by an uplift field (A) derived from an interseismic back-slip calculation (adapted from Savage, 1983; Okada, 1992) of a locked fault (B) and by ocean energy causing wave-base erosion (Anderson et al., 1999). A-B shows a reference case with a wide shelf. The vertical scale is exaggerated from -200 to 1000 m in B. The model C-D has the same parameters but a ten times greater continental uplift, and model E-F has a ten times smaller rock erodibility factor. Note that these two models both have narrower shelves, and that in model C-D, the total uplift hinge-line is displaced seaward by the fast continental uplift.

here accounts well for the first-order localization of the continental shelf (Figure 3B). The uplift hinge line anchors the edge of the shelf. The emergent shelf width in the model (and hence the distance of the shoreline to the shelf-break) is sensitive to wave energy, the erodibility of the coastal bedrock, and its rate of uplift. The numerical model illustrates the interplay of these parameters. Along the Oregon coast of Cascadia, the energy from the ocean can be reasonably assumed similar everywhere. The rock strength is bimodal with weaker mudstone of the Tyee formation to the north and somewhat stronger Franciscan melange south of Cape Blanco (Dott Jr. and Bird, 1979; Blake Jr. et al., 1985). The continental uplift rate at the coast also varies from slow in the north to faster in the south (Balco et al., 2013). Both factors co-vary and it is not possible to de-convolve their effects as they both result in a narrower shelf (Figure 3C-F). It is noteworthy that a non-uniform uplift field increasing landward allows a stabilization of the coastal region, instead of the continuous long-term net transgression or net regression resulting from coastal models with uniform uplift (Anderson et al., 1999; Snyder et al., 2002; Melnick, 2016).

Naturally, the morphology of the Cascadia margin is derived from a long geological history that is much more complicated than our model. The margin outer arc high marks the shelf break and often bounds Neogene forearc basins that have been folded, uplifted, and eroded since the Pliocene, with continuous syn-compressional deposition in some of them (Yeats et al., 1998; McNeill et al., 2000). We note that these compressional shelf basins differ from Fuller et al. (2006)'s deeper negative-α basins that develop above the locked segment when the slope of the critical wedge dips landward. We also note that the Juan de Fuca plate subducts obliquely at a 45° angle to the Cascadia margin (Kreemer et al., 2014) which causes segmentation into rotating blocks that add structural and sedimentary complexity to the margin (Kelsey and Bockheim, 1994; Personius, 1995; McCaffrey et al., 2013).

Shelf break and locking depth on a global scale

The conceptual model developed above for Cascadia should be broadly valid in any locked subduction zone. We test it below on a global compilation of the respective distances between locking depth, shelf break, and coastline following the earlier work of Ruff and Tichelaar (1996). Maps of interseismic coupling and large coseismic ruptures were collected for the major subduction systems. The downdip end of the coupled (using ~80% coupling as a threshold) and of the rupture patches were exported to Google Earth (*kml* file available in the supplementary material). In each subduction system, relative positions of the trench, the locking depth, the shelf break, and the coastline were measured along three to six profiles normal to the margin. The shelf break is identified as the transition from the continental platform edge or, in the absence of clearly defined transition to continental slope, pinned at ∼ 200 m depth. Survey profiles were positioned to capture variability in relative positions of the locking and morphological markers.

We selected 21 better resolved coseismic ruptures and interseismic coupling inversions out of 48 for a global compilation (Figure 4) following criteria detailed in text S1 and Table S1 of the supplementary information. The shelf breaks cluster around the locking depth with a mean distance of 4.7 km landward and 10th and 90th percentiles at -18 and 22 km. Coastlines, in contrast, are shifted landward with a mean distance of 43.1 km from the locking depth and 10th and 90th percentiles at 3.2 and 76.6 km. The entire dataset is presented in the supplementary Figure S2. The shelf breaks of active margins around the globe reflect the same configuration as Cascadia and support our model.

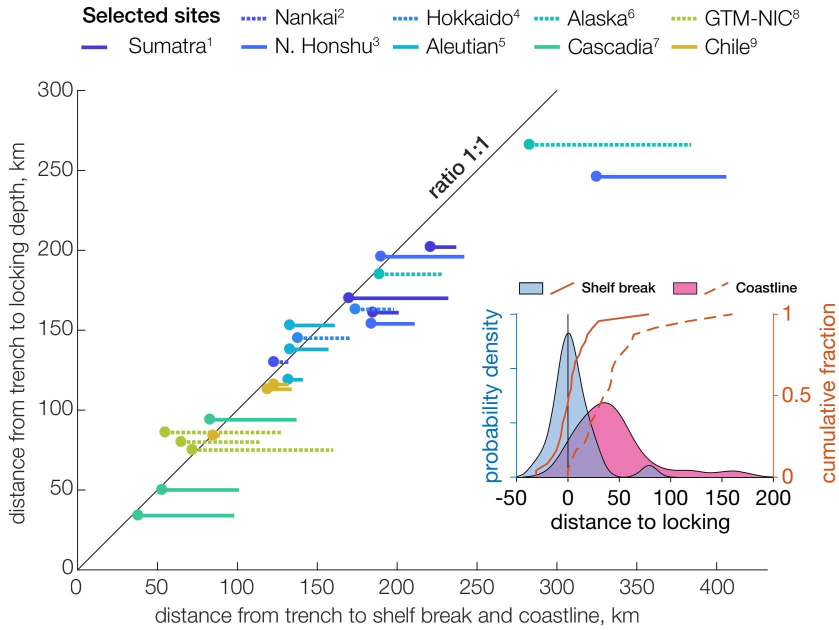

Figure 4: Position of the locking depth with respect to the shelf break and the coastline relative to the trench in selected sites (inspired by Ruff and Tichelaar (1996)). The inset distribution shows that shelf breaks are tightly distributed around the locking depth at a mean distance of 4.7 km (10th/90th percentiles at -18/22 km) while coastlines are removed and spread landward from it at a mean distance of 43.1 km (10th/90th percentiles at 3.2/76.6 km). Sources are 1: Briggs et al. (2006); Natawidjaja et al. (2007); 2: Park et al. (2002); 3: Hashimoto et al. (2009); Lay et al. (2011); 4: Hashimoto et al. (2009); 5: Johnson et al. (1994); 6: Johnson (1998); Sykes et al. (1981); 7: Burgette et al. (2009); Schmalzle et al. (2014); 8: Ye et al. (2013); 9: Lay et al. (2014); Yue et al. (2014); Li et al. (2016).

The scatter around the position of the locking depth may result from a combination of factors, chiefly among them uncertainties in the inversion of coupling and coseismic ruptures, and in the pattern of anelastic versus elastic interseismic deformation. Meanwhile, the coastlines are removed from the locking depth according to the width of the shelf. The initial observation of the co-location of coast and locking depth by Ruff and Tichelaar (1996) was primarily based on the Andean subduction, where the continental shelf is narrow to non-existent. In this case, the coastline is in close proximity to the shelf break and thereby to the locking depth as they noted. Notably, the authors identified the shelf break as possibly having "deeper physical significance [than the coastline]" (Ruff and Tichelaar, 1996).

Perspectives and conclusion

A bridge between seismic and landscape timescales

Geodetic measurements of interseismic coupling or coseismic ruptures reflect at most a few centuries of geological history. Meanwhile, the landscape records the effect of tectonics and surface processes over hundreds to thousands of individual seismic cycles spanning 100's kyr (e.g. Valensise and Ward, 1991; Willett et al., 1993; Lavé and Avouac, 2001; Avouac, 2003). Hence, on active margin if the position of the locking depth is stable — expected from a fault with a characteristic earthquake cycle, where the region locked during the interseismic period exactly delimits the extent of future earthquakes — the same domains are in net rock subsidence or rock uplift 100% of the time and the shelf break should be a sharp morphological marker (like in Cascadia potentially, Figure 5).

While the assumption of a characteristic earthquake cycle is common, interseismic coupling might also plausibly vary over several seismic cycles, leading to a more poorly defined shelf break, such as observed in Japan (Figure 5). Additionally, within the interseismic period itself, there is increasing evidence that coupling distribution could be time-dependent. The downdip end of coupling could migrate updip during the interseismic period, resulting in variable degrees of possible mismatch between coseismic reconstructions and current interseismic measurements (Thatcher, 1984; Schmalzle et al., 2014; Nishimura, 2014; Jiang and Lapusta, 2016; Wang and Tréhu, 2016; Bruhat and Segall, 2017).

Beyond temporal variations, the pattern of long term uplift depends as much on the spatial distribution of interseismic deformation as on that of coseismic displacement. Coseismic deformation can also locally over-

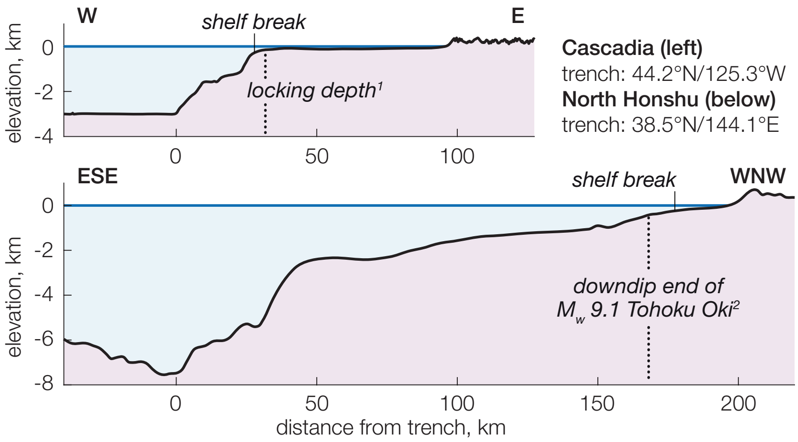

Figure 5: Profiles across the Cascadia and North Honshu margins. In Cascadia, the shelf break is a sharp and salient feature while in North Honshu the shelf break is lost in the upper continental slope. Both figures share the same scale. 1: Burgette et al. (2009); 2: Lay et al. (2011)

come interseismic deformation as in Sumatra (Sieh et al., 2008; Philibosian et al., 2014), or their respective spatial distributions could differ Penserini et al. (2017). The model proposed here opens the exploration of long-term stability or transience of interseismic locking patterns.

Critical taper and other modes of deformation

The critical taper theory (Dahlen, 1984) provides an alternative explanation for the pattern of deformation that we ascribe to the anelastic component of interseismic deformation. The deformation pattern of a critical wedge changes along variations in basal friction such that a vertical shear zone marking the transition from seaward subsidence to landward uplift can localize above the locking depth (Fuller et al., 2006; Cubas et al., 2013). However, for this hinge line to develop, the wedge has to be critical, which is a condition only met in parts of a few subduction zones (Cubas et al., 2013; Rousset et al., 2016; Koulali et al., 2018). Therefore, given the limited occurrence of critically tapered subduction zones globally, we conclude that anelastic interseismic deformation provides a more plausible explanation for the global signal of locking depths revealed by coastal geomorphology (Figure 4).

Rare deep earthquakes in the partially locked zone C *sensu* Lay et al. (2012), i.e. lower than the locking depth, have been proposed to drive coastal uplift in the Central Andes by Melnick (2016). However, it is unclear why this coseismic component alone would be the driver while all co-, post-, and interseismic stages in zone C contribute to a general deformation budget of the subduction that is dominated by the fully locked zones A-B (Lay et al., 2012).

Our modeling does not treat the subsiding part of the margin and instead assumes that a combination of deformation and sediment deposition maintains the bathymetry of the continental slope. However, evidence about deformation and sedimentation in this zone of predicted long-term subsidence supports our assumption and complements our work on the erosive part of the system. The locked domain of megathrusts has been observed to be often overlain by large forearc basins on deep sea terraces seaward of the shelf (Sugiyama, 1994; Song and Simons, 2003; Wells et al., 2003). These deep subsiding forearc basins have been attributed to subduction erosion (Wells et al., 2003), and to critical taper deformation of the inner wedge (Fuller et al., 2006; Wang and Hu, 2006; Cubas et al., 2013). If these forearc basins are indeed the depositional counterparts of erosive shelves and are driven by long-term interseismic deformation, then their stratigraphy could inform the temporal stability of the locking pattern in a manner that erosion on the shelf cannot.

Conclusion

We show that a model coupling long-term deformation derived from interseismic loading and wave erosion explains the positioning of shelf breaks above the seismic locking depths of subduction megathrusts, as observed in a global survey. The morphological expression of the seismogenic characteristics of a megathrust is particularly valuable where shelves are wide and onshore geodetic surveys accordingly limited. The submarine landscape of an active margin integrates repeated seismic cycles and bridges seismic timescales (100's yr) with those of landscape building (100's kyr). As a result, the stability, or transience, of seismic coupling is recorded in the morphology of the shelf break itself.

Acknowledgments

We thank Jean-Philippe Avouac, Emily Brodsky, Nadaya Cubas, Thorne Lay, and Baptiste Rousset for stimulating discussions. We acknowledge two anonymous reviewers for their comments. Luca Malatesta was supported by a Post.Doc Mobility fellowship of the Swiss National Science Foundation
(P2SKP2_168328).

References

K. Aki. Scaling law of seismic spectrum. *Journal of Geophysical Research: Planets*, 72(4):1217–1231, 1967.

R. W. Allmendinger, J. P. Loveless, M. E. Pritchard, and B. Meade. From decades to epochs: Spanning the gap between geodesy and structural geology of active mountain belts. *Journal Of Structural Geology*, 31(11):1409–1422, Nov. 2009.

R. S. Anderson, A. L. Densmore, and M. A. Ellis. The generation and degradation of marine terraces. *Basin Research*, 11(1):7–19, Mar. 1999.

J.-P. Avouac. Mountain building, erosion, and the seismic cycle in the Nepal Himalaya. *Advances in Geophysics*, 2003.

G. Balco, N. J. Finnegan, A. Gendaszek, J. O. H. Stone, and N. Thompson. Erosional response to northward-propagating crustal thickening in the coastal ranges of the U.S. Pacific Northwest. *American Journal Of Science*, 313(8):790–806, Oct. 2013.

M. C. Blake Jr., A. S. Jayko, and R. J. McLaughlin. Tectonostratigraphic terranes of the northern Coast Ranges, California. *Tectonostratigraphic Terranes of the Circum-Pacific Region, Earth Science Series*, 1, 1985.

W. C. Bradley and G. B. Griggs. Form, genesis, and deformation of central California wave-cut platforms. *Geological Society of America Bulletin*, 87(3): 433–449, Mar. 1976.

R. W. Briggs, K. Sieh, A. J. Meltzner, D. Natawidjaja, J. Galetzka, B. W. Suwargadi, Y. J. Hsu, M. Simons, N. Hananto, I. Suprihanto, D. Prayudi, J.-P. Avouac, L. Prawirodirdjo, and Y. Bock. Deformation and slip along the Sunda Megathrust in the great 2005 Nias-Simeulue earthquake. *Science*, 311(5769):1897–1901, 2006.

B. A. Brooks, M. Bevis, K. Whipple, J. R. Arrowsmith, J. Foster, T. Zapata, E. Kendrick, E. Minaya, A. Echalar, M. Blanco, P. Euillades, M. Sandoval, and R. J. Smalley. Orogenic-wedge deformation and potential for great earthquakes in the central Andean backarc. *Nature Geoscience*, 4(6):380–383, May 2011.

L. Bruhat and P. Segall. Coupling on the northern Cascadia subduction zone from geodetic measurements and physics-based models. *Journal of Geophysical Research*, 121(11):8297–8314, Nov. 2016.

L. Bruhat and P. Segall. Deformation rates in northern Cascadia consistent with slow updip propagation of deep interseismic creep. *Geophysical Journal International*, 211(1):427–449, July 2017.

R. J. Burgette, R. J. Weldon II, and D. A. Schmidt. Interseismic uplift rates for western Oregon and along-strike variation in locking on the Cascadia subduction zone. *Journal of Geophysical Research*, 114(B1):TC3009–24, Jan. 2009.

R. Bürgmann and D. Chadwell. Seafloor Geodesy. *Annual Review Of Earth And Planetary Sciences*, 42(1):509–534, May 2014.

R. Cattin and J.-P. Avouac. Modeling mountain building and the seismic cycle in the Himalaya of Nepal. *Journal of Geophysical Research*, 105:13389–13407, 2000.

M. Chlieh, J.-P. Avouac, K. Sieh, D. H. Natawidjaja, and J. Galetzka. Heterogeneous coupling of the Sumatran megathrust constrained by geodetic and paleogeodetic measurements. *Journal of Geophysical Research*, 113 (B5):2018–31, May 2008.

F. Crameri. Geodynamic diagnostics, scientific visualisation and StagLab 3.0. *Geoscientific Model Development*, 11 (6):2541–2562, 2018.

N. Cubas, J.-P. Avouac, P. Souloumiac, and Y. Leroy. Megathrust friction determined from mechanical analysis of the forearc in the Maule earthquake area. *Earth and Planetary Science Letters*, 381(C):92–103, Nov. 2013.

F. A. Dahlen. Noncohesive Critical Coulomb Wedges - an Exact Solution. *Journal of Geophysical Research*, 89: 125–133, 1984.

R. H. Dott Jr. and K. J. Bird. Sand Transport Through Channels Across an Eocene Shelf and Slope in Southwestern Oregon, U.S.A. In *Geology of Continental Slopes*, pages 327–342. SEPM (Society for Sedimentary Geology), 1979.

H. Dragert, K. L. Wang, and T. S. James. A silent slip event on the deeper Cascadia subduction interface. *Science*, 292 (5521):1525–1528, 2001.

C. Fuller, S. D. Willett, and M. T. Brandon. Formation of forearc basins and their influence on subduction zone earthquakes. *Geology*, 34(2):65–68, 2006.

C. Goldfinger, L. D. Kulm, R. S. Yeats, B. Appelgate, M. E. MacKay, and G. F. Moore. Transverse structural trends along the Oregon convergent margin: Implications for Cascadia earthquake potential and crustal rotations. *Geology*, 20(2):141–144, Feb. 1992.

C. Hashimoto, A. Noda, T. Sagiya, and M. Matsu'ura. Interplate seismogenic zones along the Kuril-Japan trench inferred from GPS data inversion. *Nature Geoscience*, 2(2):141–144, Jan. 2009.

R. D. Hyndman and K. Wang. The Rupture Zone of Cascadia Great Earthquakes From Current Deformation and the Thermal Regime. *Journal of Geophysical Research*, 100(B11):22133–22154, 1995.

T. S. James, E. J. Gowan, I. Wada, and K. Wang. Viscosity of the asthenosphere from glacial isostatic adjustment and subduction dynamics at the northern Cascadia subduction zone, British Columbia, Canada. *Journal of Geophysical Research-Solid Earth and Planets*, 114(B4):536–13, Apr. 2009.

J. Jiang and N. Lapusta. Deeper penetration of large earthquakes on seismically quiescent faults. *Science*, 352(6291): 1293–1297, June 2016.

J. M. Johnson. Heterogeneous Coupling Along Alaska-Aleutians as Inferred From Tsunami, Seismic, and Geodetic Inversions. In *Tsunamigenic Earthquakes and Their Consequences*, pages 1–116. Elsevier, 1998.

J. M. Johnson, Y. Tanioka, L. J. Ruff, K. Satake, H. Kanamori, and L. R. Sykes. The 1957 great Aleutian earthquake Pure Applied Geophysics, 142 (1), 1994, pp 3–28. *Pure and Applied Geophysics*, 142(1):3–28, Dec. 1994.

R. V. S. Kanda and M. Simons. An elastic plate model for interseismic deformation in subduction zones. *Journal of Geophysical Research: Planets*, 115 (B3), 2010.

H. M. Kelsey and J. G. Bockheim. Coastal landscape evolution as a function of eustasy and surface uplift rate, Cascadia margin, southern Oregon. *Geological Society of America Bulletin*, 106(6): 840–854, June 1994.

A. Koulali, S. McClusky, P. Cummins, and P. Tregoning. Wedge geometry, frictional properties and interseismic coupling of the Java megathrust. *Tectonophysics*, 734-735:89–95, June 2018.

C. Kreemer, G. Blewitt, and E. C. Klein. A geodetic plate motion and Global Strain Rate Model. *Geochemistry Geophysics Geosystems*, 15(10):3849–3889, Oct. 2014.

R. D. Krogstad, D. A. Schmidt, R. J. Weldon, and R. J. Burgette. Constraints on accumulated strain near the ETS zone along Cascadia. *Earth and Planetary Science Letters*, 439(C):109–116, Apr. 2016.

J. Lavé and J.-P. Avouac. Fluvial incision and tectonic uplift across the Himalayas of central Nepal. *Journal of Geophysical Research*, 106(B11): 26561–26,591, Jan. 2001.

T. Lay, C. J. Ammon, H. Kanamori, L. Xue, and M. J. Kim. Possible large near-trench slip during the 2011 M_w9.0 off the Pacific coast of Tohoku Earthquake. *Earth, Planets and Space*, 63 (7):687–692, Sept. 2011.

T. Lay, H. Kanamori, C. J. Ammon, K. D. Koper, A. R. Hutko, L. Ye, H. Yue, and T. M. Rushing. Depth-varying rupture properties of subduction zone megathrust faults. *Journal of Geophysical Research*, 117(B4):n/a–n/a, Apr. 2012.

T. Lay, H. Yue, E. E. Brodsky, and C. An. The 1 April 2014 Iquique, Chile, M_w8.1 earthquake rupture sequence. *Geophysical Research Letters*, 41(11):3818–3825, June 2014.

X. Le Pichon, S. Mazzotti, P. Henry, and M. Hashimoto. Deformation of the Japanese Islands and seismic coupling: an interpretation based on GSI permanent GPS observations. *Geophysical Journal International*, 134(2):501–514, Aug. 1998.

L. Li, T. Lay, K. F. Cheung, and L. Ye. Joint modeling of teleseismic and tsunami wave observations to constrain the 16 September 2015 Illapel, Chile, M_w8.3 earthquake rupture process. *Geophysical Research Letters*, 43 (9):4303–4312, May 2016.

J. P. Loveless and R. W. Allmendiger. Implications of elastic dislocation modeling on permanent deformation in the Northern Chilean forearc. In *International Symposium on Andean Geodynamics*, pages 454–457, Barcelona, 2005.

P. M. Mai and G. C. Beroza. Source Scaling Properties from Finite-Fault-Rupture Models. *Bulletin of the Seismological Society of America*, 90(3): 604–615, June 2000.

S. Mazzotti, X. Le Pichon, P. Henry, and S.-I. Miyazaki. Full interseismic locking of the Nankai and Japan-west Kurile subduction zones: An analysis of uniform elastic strain accumulation in Japan constrained by permanent GPS. *Journal of Geophysical Research*, 105(B6):13159–13177, June 2000.

R. McCaffrey, A. I. Qamar, R. W. King, R. Wells, G. Khazaradze, C. A. Williams, C. W. Stevens, J. J. Vollick, and P. C. Zwick. Fault locking, block rotation and crustal deformation in the Pacific Northwest. *Geophysical Journal International*, 169(3): 1315–1340, June 2007.

R. McCaffrey, R. W. King, S. J. Payne, and M. Lancaster. Active tectonics of northwestern U.S. inferred from GPS-derived surface velocities. *Journal of Geophysical Research*, 118(2):709–723, Feb. 2013.

L. C. McNeill, C. Goldfinger, L. D. Kulm, and R. S. Yeats. Tectonics of the Neogene Cascadia forearc basin: Investigations of a deformed late Miocene unconformity. *Geological Society of America Bulletin*, 112(8):1209–1224, Aug. 2000.

D. Melnick. Rise of the central Andean coast by earthquakes straddling the Moho. *Nature Geoscience*, 9(5):401–407, Mar. 2016.

M. Metois, A. Socquet, and C. Vigny. Interseismic coupling, segmentation and mechanical behavior of the central Chile subduction zone. *Journal of Geophysical Research*, 117(B3):40–16, Mar. 2012.

D. H. Natawidjaja, K. Sieh, J. Galetzka, B. W. Suwargadi, H. Cheng, R. L. Edwards, and M. Chlieh. Interseismic deformation above the Sunda Megathrust recorded in coral microatolls of the Mentawai islands, West Sumatra. *Journal of Geophysical Research-Solid Earth and Planets*, 112(B2):1897–27, Feb. 2007.

T. Nishimura. Pre-, Co-, and Post-Seismic Deformation of the 2011 Tohoku-Oki Earthquake and its Implication to a Paradox in Short-Term and Long-Term Deformation. *Journal of Disaster Research*, 9(3):294–302, June 2014.

T. Nishimura, T. Hirasawa, S. Miyazaki, T. Sagiya, T. Tada, S. Miura, and K. Tanaka. Temporal change of interplate coupling in northeastern Japan during 1995–2002 estimated from continuous GPS observations. *Geophysical Journal International*, 157(2):901–916, May 2004.

K. Obara. Nonvolcanic deep tremor associated with subduction in southwest Japan. *Science*, 296(5573):1679–1681, 2002.

Y. Okada. Internal deformation due to shear and tensile faults in a half-space. *Bulletin of the Seismological Society of America*, 82(2):1018–1040, Apr. 1992.

J.-O. Park, T. Tsuru, S. Kodaira, P. R. Cummins, and Y. Kaneda. Splay Fault Branching Along the Nankai Subduction Zone. *Science*, 297(5584):1157–1160, Aug. 2002.

B. D. Penserini, J. J. Roering, and A. Streig. A morphologic proxy for debris flow erosion with application to the earthquake deformation cycle, Cascadia Subduction Zone, USA. *Geomorphology*, 282(C):150–161, Apr. 2017.

S. F. Personius. Late Quaternary stream incision and uplift in the forearc of the Cascadia subduction zone, western Oregon - Personius - 1995 - Journal of Geophysical Research: Solid Earth - Wiley Online Library. *Journal of Geophysical Research*, 1995.

B. Philibosian, K. Sieh, J.-P. Avouac, D. H. Natawidjaja, H.-W. Chiang, C.-C. Wu, H. Perfettini, C.-C. Shen, M. R. Daryono, and B. W. Suwargadi. Rupture and variable coupling behavior of the Mentawai segment of the Sunda megathrust during the supercycle culmination of 1797 to 1833. *Journal of Geophysical Research*, 119(9):7258–7287, Sept. 2014.

M. Rosenau, J. Lohrmann, and O. Oncken. Shocks in a box: An analogue model of subduction earthquake cycles with application to seismotectonic forearc evolution. *Journal of Geophysical Research*, 114(B1):183–20, Jan. 2009.

B. Rousset, C. Lasserre, N. Cubas, S. Graham, M. Radiguet, C. DeMets, A. Socquet, M. Campillo, V. Kostoglodov, E. Cabral-Cano, N. Cotte, and A. Walpersdorf. Lateral Variations of Interplate Coupling along the Mexican Subduction Interface: Relationships with Long-Term Morphology and Fault Zone Mechanical Properties. *Pure and Applied Geophysics*, 173(10): 3467–3486, 2016.

L. J. Ruff and B. W. Tichelaar. What Controls the Seismogenic Plate Interface in Subduction Zones? In *Geophysical Monograph Series*, pages 105–111. American Geophysical Union, 1996.

T. Sagiya. Interplate coupling in the Tokai District, central Japan, deduced from continuous GPS data. *Geophysical Research Letters*, 26(15):2315–2318, 1999.

M. Saillard, L. Audin, B. Rousset, J.-P. Avouac, M. Chlieh, S. R. Hall, L. Husson, and D. L. Farber. From the seismic cycle to long-term deformation: linking seismic coupling and Quaternary coastal geomorphology along the Andean megathrust. *Tectonics*, 36(2): 241–256, Feb. 2017.

K. Satake, K. Shimazaki, Y. Tsuji, and K. Ueda. Time and size of a giant earthquake in Cascadia inferred from Japanese tsunami records of January 1700. *Nature*, 379(6562):246–249, Jan. 1996.

K. Satake, K. L. Wang, and B. F. Atwater. Fault slip and seismic moment of the 1700 Cascadia earthquake inferred from Japanese tsunami descriptions. *Journal of Geophysical Research*, 108(B11), 2003.

J. C. Savage. A Dislocation Model of Strain Accumulation and Release at a Subduction Zone. *Journal of Geophysical Research-Solid Earth and Planets*, 88(NB6):4984–4996, 1983.

G. M. Schmalzle, R. McCaffrey, and K. C. Creager. Central Cascadia subduction zone creep. *Geochemistry Geophysics Geosystems*, 15(4):1515–1532, Apr. 2014.

K. Sieh, D. H. Natawidjaja, A. J. Meltzner, C. C. Shen, H. Cheng, K. S. Li, B. W. Suwargadi, J. Galetzka, B. Philibosian, and R. L. Edwards. Earthquake Supercycles Inferred from Sea-Level Changes Recorded in the Corals of West Sumatra. *Science*, 322 (5908):1674–1678, Dec. 2008.

M. Simoes, J.-P. Avouac, R. Cattin, and P. Henry. The Sumatra subduction zone: A case for a locked fault zone extending into the mantle. *Journal of Geophysical Research: Planets*, 109 (B10), 2004.

N. P. Snyder, K. X. Whipple, G. E. Tucker, and D. J. Merritts. Interactions between onshore bedrock-channel incision and nearshore wave-base erosion forced by eustasy and tectonics. *Basin Research*, 14(2):105–127, June 2002.

T.-R. A. Song and M. Simons. Large Trench-Parallel Gravity Variations Predict Seismogenic Behavior in Subduction Zones. *Science*, 301(5633):630–633, Aug. 2003.

R. M. Spratt and L. E. Lisiecki. A Late Pleistocene sea level stack. *Climate of the Past*, 12(4):1079–1092, 2016.

V. L. Stevens and J.-P. Avouac. Interseismic coupling on the main Himalayan thrust. *Geophysical Research Letters*, 42(14):5828–5837, 2015.

Y. Sugiyama. Neotectonics of Southwest Japan due to the right-oblique subduction of the Philippine Sea plate. *Geofísica Internacional*, 33(1):53–76, 1994.

L. R. Sykes, J. B. Kisslinger, L. House, J. N. Davies, and K. H. Jacob. Rupture Zones and Repeat Times of Great Earthquakes Along the Alaska-Aleutian ARC, 1784–1980. In D. W. Simpson and P. G. Richards, editors, *Earthquake Prediction An International Review*, pages 73–80. American Geophysical Union, Washington, D. C., 1981.

W. Thatcher. The Earthquake Deformation Cycle at the Nankai Trough, Southwest Japan. *Journal of Geophysical Research-Solid Earth and Planets*, 89(NB5):3087–3101, 1984.

G. Valensise and S. N. Ward. Long-Term Uplift of the Santa-Cruz Coastline in Response to Repeated Earthquakes Along the San-Andreas Fault. *Bulletin of the Seismological Society of America*, 81(5):1694–1704, Oct. 1991.

Y. van Dinther, T. V. Gerya, L. A. Dalguer, P. M. Mai, G. Morra, and D. Giardini. The seismic cycle at subduction thrusts: Insights from seismo-thermo-mechanical models. *Journal of Geophysical Research*, 118(12):6183–6202, Dec. 2013.

J. Vergne, R. Cattin, and J.-P. Avouac. On the use of dislocations to model interseismic strain and stress build-up at intracontinental thrust faults. *Geophysical Journal International*, 147(1): 155–162, Sept. 2001.

K. Wang and Y. Hu. Accretionary prisms in subduction earthquake cycles: The theory of dynamic Coulomb wedge. *Journal of Geophysical Research*, 111 (B6):n/a–n/a, June 2006.

K. Wang and A. M. Tréhu. Invited review paper: Some outstanding issues in the study of great megathrust earthquakes—The Cascadia example. *Journal of Geodynamics*, 98:1–18, Aug. 2016.

K. Wang, R. Wells, S. Mazzotti, R. D. Hyndman, and T. Sagiya. A revised dislocation model of interseismic deformation of the Cascadia subduction zone. *Journal of Geophysical Research*, 108 (B1):1085–13, Jan. 2003.

R. E. Wells, R. J. Blakely, Y. Sugiyama, D. W. Scholl, and P. A. Dinterman. Basin-centered asperities in great subduction zone earthquakes: A link between slip, subsidence, and subduction erosion? *Journal of Geophysical Research: Planets*, 108(B10), 2003.

S. D. Willett, C. Beaumont, and P. Fullsack. Mechanical Model for the Tectonics of Doubly Vergent Compressional Orogens. *Geology*, 21(4):371–374, 1993.

L. Ye, T. Lay, and H. Kanamori. Large earthquake rupture process variations on the Middle America megathrust. *Earth and Planetary Science Letters*, 381(C):147–155, Nov. 2013.

R. S. Yeats, L. D. Kulm, C. Goldfinger, and L. C. McNeill. Stonewall anticline: An active fold on the Oregon continental shelf. *Geological Society of America Bulletin*, 110(5):572–587, May 1998.

T. Yoshikawa. Seismic Crustal Deformation and its Relation to Quaternary Tectonic Movement on the Pacific Coast of Southwest Japan. *The Quaternary Research (Daiyonki-Kenkyu)*, 7(4):157–170, Dec. 1968.

T. Yoshikawa, S. Kaizuka, and Y. Ôta. *The landforms of Japan /*. University of Tokyo Press, Tokyo, 1981.

S. Yoshioka, T. Yabuki, T. Sagiya, T. Tada, and M. Matsu'ura. Interplate coupling and relative plate motion in the Tokai district, central Japan, deduced from geodetic data inversion using ABIC. *Geophysical Journal International*, 113:607–621, 1993.

H. Yue, T. Lay, L. Rivera, C. An, C. Vigny, X. Tong, and J. C. Báez Soto. Localized fault slip to the trench in the 2010 Maule, Chile $M_w = 8.8$ earthquake from joint inversion of high-rate GPS, teleseismic body waves, InSAR, campaign GPS, and tsunami observations. *Journal of Geophysical Research*, 119(10):7786–7804, Oct. 2014.

Supplementary information for the pre-print article: Co-location of the downdip end of seismic locking and the continental shelf break

Luca C. Malatesta[1,2,*], Lucile Bruhat[3], Noah J. Finnegan[1]

[1]Department of Earth and Planetary Sciences, University of California Santa Cruz, Santa Cruz, California, USA.
[2]Institute of Earth Surface Dynamics, University of Lausanne, Lausanne, Switzerland.
[3]Department of Geology, École Normale Supérieure, Paris, France
*corresponding author: luca.malatesta@unil.ch

Contents of this file

1. Text S1
2. Figures S1 to S2
3. Table S1
4. Description of *kml* file

Text S1: Selection criteria for the compilation

We established selection criteria to use only the most reliable locking depth solutions in out global dataset. They are detailed below and supplementary Table 1 details which 21 inversions out of 48 total were selected.

Seismic ruptures need to be large enough to outline the downdip end of coupling ($\sim M_w > 7$, *Lay et al.*, 2012). We ignore large seismic ruptures from historical catalogues that are only vaguely outlined and instead rely on ruptures that were heavily instrumented (*Yue et al.*, 2014).

At sites where no large earthquake was recorded, coupling is determined based on interseismic deformation recorded by GNSS stations (located almost entirely onshore). In cases of well resolved co- and interseismic solutions, inversions from coseismic ruptures were selected over interseismic inversions. We select interseismic locking depth solutions if models can demonstrably resolve coupling offshore and if an agreement exists between different studies. Spatial resolution is mostly determined by the density and spatial distribution of geodetic measurements, and their associated uncertainties (*Wang and Tréhu*, 2016). Uncertainties over the locking depth estimate increase for wider continental shelves due larger separation between onshore stations and the locked region (e.g. *LaFemina et al.*, 2009; *Franco et al.*, 2012, in Central America). For lack of a simple selection criterion, we ignore locations where locking depth solutions derived from similar datasets by different authors vary greatly.

Four subduction zones are excluded from the reduced compilation because their geometry or coastal processes do not follow our conceptual model. The northern Kuril subduction, under Kamtchatka, dips steeply, placing arc volcanism so close to the trench that the margin is aggradational as volcanoes encroach on the sea (*Bürgmann*, 2005). The Gorda micro-plate in the southern Cascadia subduction zone is a very young oceanic plate (∼3Ma, *Stock and Lee*, 2010) whose slab deforms heavily under the active margin and the long-term interseismic deformation is likely to vary on a much faster timescale than that of the establishment of the submarine landscape. At the junction between Central and South America, vertical motion above the Costa Rica subduction zone is controlled by episodic forcings that reflect the subduction of structural and geological complexities (*Edwards et al.*, 2018). Finally, the Colombian coastline is aggradational, as it appears that the sediment flux reaching the coast suffices to overcome coastal erosion and build land.

Description of *kml* file

The *kml* file attached to this contribution contains the traces of all locking depths imported from the literature (see Table S1) and shelf break outlines as well as the positions of the profiles used to build Figure 4 and Figure S2.

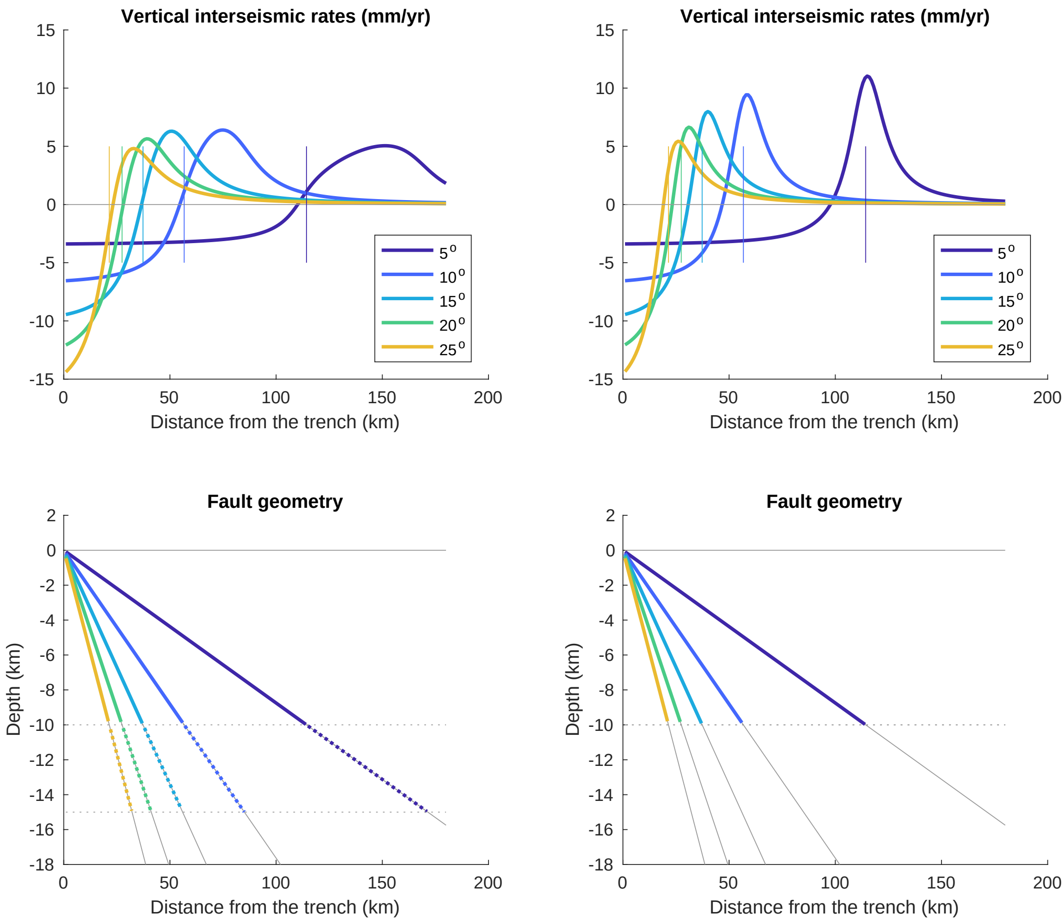

Figure 1: Left: relationship between the uplift hinge line and the locking depth for a fault with transitional locking (from 10 to 15 km) at varying dip angles. Right: same as left but without transitional locking. The uplift hinge line is most removed from the position of the locking depth for gently sloping faults without transitional locking. A zone of transitional locking is however expected in most if not all locations.

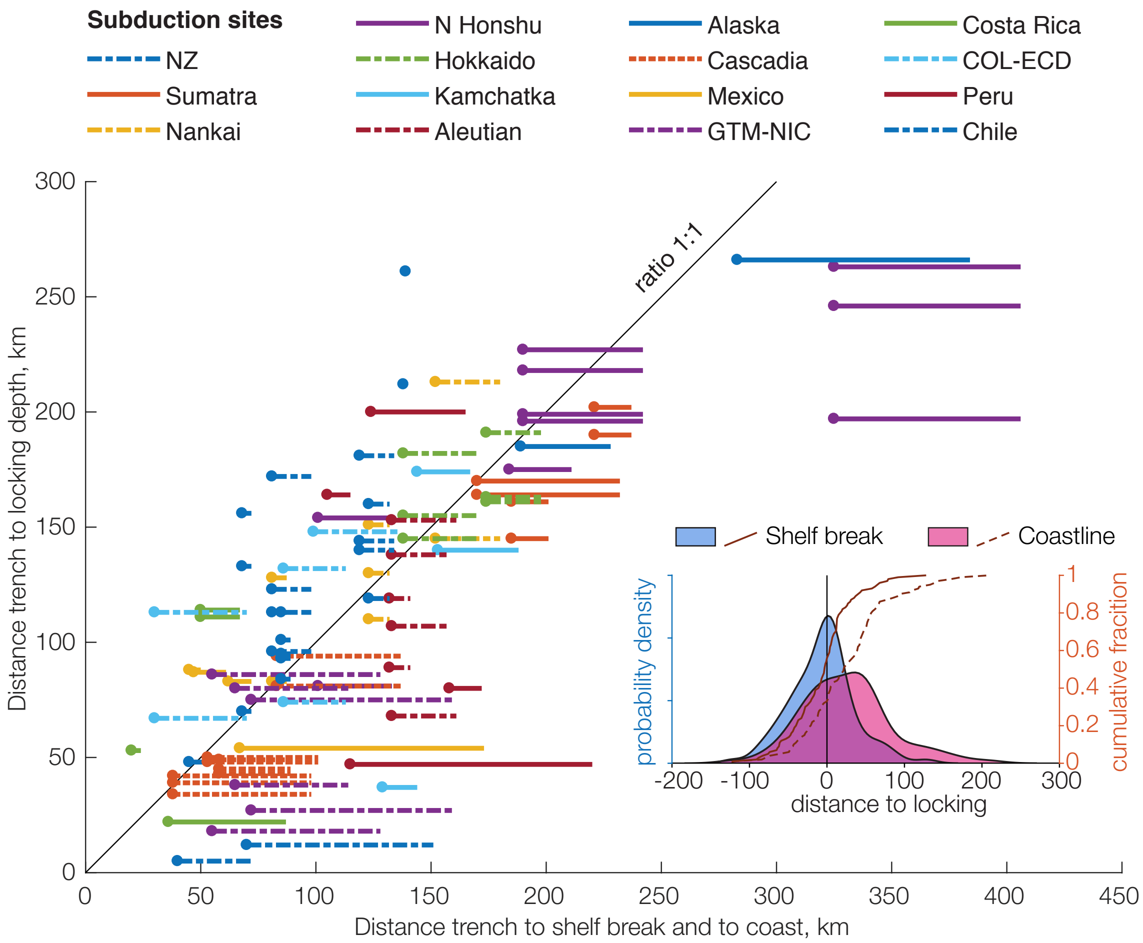

Figure 2: Position of the locking depth with respect to the shelf break and the coastline for the entire dataset collected here. The sites that have multiple locking depth solutions are aligned vertically. Details and sources of the data are listed in Table 1. For the entire dataset, the mean distance between shelf break and locking depth is -6.18 km with 10^{th} and 90^{th} percentiles of -61.5 km and 40 km respectively, and the mean distance between coastline and locking depth of 25.17 km with 10^{th} and 90^{th} percentiles of -43 km and 93 km respectively.

Table 1: List of measurements on profiles across subduction zones. The latitude/longitude coordinates indicate the intersection between profile and subduction trench (or deformation front). The Method column reflects if locking depth is identified from inversion of GPS or leveling (LVL) data, from slab isotherms (isoT), or from the inversion of coseismic ruptures (EQ). The selection columns reflects whether the solution was selected for Figure 4 of the main text along side a rationale for the choice: *creep*, the fault is creeping; *co>inter*: coseismic solutions are favored over interseismic ones (also used for all profiles of subductions where one resolved coseismic rupture contradicts an interseismic solution); *isoT*, solutions based on isotherm estimates are ignored; *default*, best solution and others are ignored; *volc. coast*, the coast is not erosional but built up by volcanoes; *island*, the coastline is offset from the continent by an island; *tecto.*, local tectonics deviate strongly from a standard subduction geometry (due to strike-slip components, slab age or dip angle); *equiv.*, one solution is picked among equivalent ones; *resolut.*, the resolution of the inversion is too low; *deposit.*, the coast is not erosional but built up by sediments; *contrad.*, different solutions contradict each other.

Subduction		**Dist. trench to... [km]**					
transect	**Lat./Lon.**	**shelf**	**coast**	**locking**	**Method**	**Reference**	**Selection**
Hikurangi 1	-41.86/175.89	45	52	48	GPS	*Wallace* (2004)	No (creep)
Hikurangi 2	-39.80/178.63	70	151	12	GPS	*Wallace* (2004)	No (creep)
Hikurangi 3	-38.51/179.11	40	72	5	GPS	*Wallace* (2004)	No (creep)
Sumatra 1	-4.28/100.18	170	232	164	GPS	*Chlieh et al.* (2008)	No (co>inter)
”	”	”	”	170	EQ	*Natawidjaja et al.* (2007)	Yes (co>inter)
Sumatra 2	-2.42/98.65	221	237	190	GPS	*Chlieh et al.* (2008)	No (co>inter)
”	”	”	”	202	EQ	*Natawidjaja et al.* (2007)	Yes (co>inter)
Sumatra 3	0.76/96.81	185	201	145	GPS	*Chlieh et al.* (2008)	No (co>inter)
”	”	”	”	213	EQ	*Briggs et al.* (2006)	Yes (co>inter)
Nankai 1	32.03/134.37	152	180	145	isoT	*Hyndman et al.* (1995)	No (isoT)
”	”	”	”	213	GPS	*Loveless and Meade* (2010)	No (co>inter)
Nankai 2	32.74/136.10	81	88	83	isoT	*Hyndman et al.* (1995)	No (isoT)
”	”	”	”	128	GPS	*Loveless and Meade* (2010)	No (co>inter)
Nankai 3	33.18/137.22	123	132	110	isoT	*Hyndman et al.* (1995)	No (isoT)
”	”	”	”	151	GPS	*Loveless and Meade* (2010)	No (co>inter)
”	”	”	”	130	EQ	*Park et al.* (2002)	Yes (co>inter)
N. Honshu 1	35.24/142.22	101	133	154	isoT	*Hyndman et al.* (1995)	No (isoT)
”	”	”	”	81	GPS	*Loveless and Meade* (2010)	No (co>inter)
N. Honshu 2	37.34/143.72	190	242	199	isoT	*Hyndman et al.* (1995)	No (co>inter)
”	”	”	”	218	GPS	*Loveless and Meade* (2010)	No (co>inter)
”	”	”	”	227	GPS	*Hashimoto et al.* (2009)	No (co>inter)
”	”	”	”	196	EQ	*Lay et al.* (2011)	Yes (co>inter)
N. Honshu 3	39.96/144.33	184	211	175	isoT	*Hyndman et al.* (1995)	No (isoT)
”	”	”	”	154	GPS	*Hashimoto et al.* (2009)	Yes (default)
N. Honshu 4	40.61/144.53	325	406	197	isoT	*Hyndman et al.* (1995)	No (isoT)
”	”	”	”	263	GPS	*Loveless and Meade* (2010)	No (co>inter)

Table 1: continued from previous page.

Subduction transect	Lat./Lon.	Dist. trench to... [km] shelf	coast	locking	Method	Reference	Selection
”	”	”	”	246	GPS	*Hashimoto et al.* (2009)	Yes (default)
Hokkaido 1	41.30/145.14	174	198	161	isoT	*Hyndman et al.* (1995)	No (isoT)
”	”	”	”	191	GPS	*Loveless and Meade* (2010)	No (co>inter)
”	”	”	”	186	GPS	*Hashimoto et al.* (2009)	Yes (default)
Hokkaido 2	41.88/146.43	138	171	155	isoT	*Hyndman et al.* (1995)	No (isoT)
”	”	”	”	182	GPS	*Loveless and Meade* (2010)	No (co>inter)
”	”	”	”	172	GPS	*Hashimoto et al.* (2009)	Yes (default)
Kamchatka 1	51.12/160.26	144	167	174	GPS	*Bürgmann* (2005)	No (volc. coast)
Kamchatka 2	53.36/162.62	153	188	140	GPS	*Bürgmann* (2005)	No (volc. coast)
Kamchatka 3	54.87/163.68	129	144	37	GPS	*Bürgmann* (2005)	No (volc. coast)
Aleutian 1	50.39/177.95	132	141	89	GPS	*Cross and Freymueller* (2007)	No (co>inter)
”	”	”	”	119	EQ	*Johnson et al.* (1994)	Yes (co>inter)
Aleutian 2	50.56/-175.43	133	157	107	GPS	*Cross and Freymueller* (2007)	No (co>inter)
”	”	”	”	138	EQ	*Johnson et al.* (1994)	Yes (co>inter)
Aleutian 3	50.72/-173.64	133	161	68	GPS	*Cross and Freymueller* (2007)	No (co>inter)
”	”	”	”	153	EQ	*Johnson et al.* (1994)	Yes (co>inter)
Alaska 1	54.28/-156.82	189	228	185	EQ	*Johnson* (1998)	Yes (default)
Alaska 2	56.18/-151.56	138	138	212	EQ	*Sykes et al.* (1981)	No (island)
Alaska 3	57.25/-148.56	283	384	266	EQ	*Sykes et al.* (1981)	Yes (default)
Alaska 4	58.83/-146.18	139	139	261	EQ	*Sykes et al.* (1981)	No (tecto.)
Cascadia 1	48.43/-126.85	53	101	48	GPS	*Wang et al.* (2003)	No (equiv.)
”	”	”	”	50	GPS	*McCaffrey et al.* (2007)	No (equiv.)
”	”	”	”	50	GPS	*Schmalzle et al.* (2014)	Yes (equiv.)
Cascadia 2	46.67/-125.89	83	137	81	GPS	*Wang et al.* (2003)	No (equiv.)
”	”	”	”	50	GPS	*McCaffrey et al.* (2007)	No (equiv.)
”	”	”	”	94	GPS	*Schmalzle et al.* (2014)	Yes (equiv.)
Cascadia 3	44.33/-125.33	38	98	39	GPS	*Wang et al.* (2003)	No (equiv.)
”	”	”	”	50	GPS	*McCaffrey et al.* (2007)	No (equiv.)
”	”	”	”	42	GPS	*Schmalzle et al.* (2014)	No (equiv.)

Table 1: continued from previous page.

Subduction transect	Lat./Lon.	Dist. trench to... [km] shelf	coast	locking	Method	Reference	Selection
"	"	"	"	34	LVL	*Burgette et al.* (2009)	Yes (equiv.)
Cascadia 4	42.017/-125.27	58	89	43	GPS	*Wang et al.* (2003)	No (tecto.)
"	"	"	"	50	GPS	*McCaffrey et al.* (2007)	No (tecto.)
"	"	"	"	45	GPS	*Schmalzle et al.* (2014)	No (tecto.)
"	"	"	"	49	LVL	*Burgette et al.* (2009)	No (tecto.)
Mexico 1	17.54/-103.17	62	72	83	EQ	*Radiguet et al.* (2012)	No (tecto.)
Mexico 2	16.16/-99.69	47	61	87	EQ	*Radiguet et al.* (2012)	No (tecto.)
Mexico 3	15.30/-96.95	45	50	88	EQ	*Radiguet et al.* (2012)	No (tecto.)
Mexico 4	14.43/-94.39	67	173	54	GPS	*Franco et al.* (2012)	No (resolut.)
GTM to NIC 1	13.31/-92.35	65	115	38	GPS	*LaFemina et al.* (2009)	No (resolut.)
"	"	"	"	80	EQ	*Ye et al.* (2013)	Yes (default)
GTM to NIC 2	11.84/-88.79	72	160	27	GPS	*LaFemina et al.* (2009)	No (resolut.)
"	"	"	"	75	EQ	*Ye et al.* (2013)	Yes (default)
GTM to NIC 3	10.95/-87.33	55	128	18	GPS	*LaFemina et al.* (2009)	No (resolut.)
"	"	"	"	86	EQ	*Ye et al.* (2013)	Yes (default)
Costa Rica 1	9.41/-85.92	50	67	114	GPS	*LaFemina et al.* (2009)	No (tecto.)
"	"	"	"	111	EQ	*Ye et al.* (2013)	No (tecto.)
Costa Rica 2	8.57/-84.27	36	87	22	GPS	*LaFemina et al.* (2009)	No (tecto.)
Costa Rica 3	8.23/-83.48	20	24	53	GPS	*LaFemina et al.* (2009)	No (tecto.)
COL - ECD 1	3.83/-78.58	99	136	148	EQ	*Kanamori and McNally* (1982)	No (deposit.)
COL - ECD 2	1.74/-79.95	86	113	132	EQ	*Kanamori and McNally* (1982)	No (deposit.)
"	"	"	"	74	GPS	*Nocquet et al.* (2014)	No (deposit.)
COL - ECD 3	-0.03/-80.99	30	70	113	EQ	*Kanamori and McNally* (1982)	No (deposit.)
"	"	"	"	67	GPS	*Nocquet et al.* (2014)	No (deposit.)
Peru 1	-9.01/-80.81	115	220	47	GPS	*Nocquet et al.* (2014)	No (resolut.)
Peru 2	-12.92/-78.34	124	165	200	GPS	*Nocquet et al.* (2014)	No (resolut.)
Peru 3	-17.78/-73.78	105	115	164	GPS	*Chlieh et al.* (2011)	No (resolut.)

Table 1: continued from previous page.

Subduction transect	**Lat./Lon.**	**Dist. trench to... [km]**			**Method**	**Reference**	**Selection**
		shelf	**coast**	**locking**			
Peru 4	-19.15/-71.85	158	172	80	GPS	*Chlieh et al.* (2011)	No (resolut.)
Chile 1	-19.90/-71.39	123	132	119	GPS	*Chlieh et al.* (2011)	No (co>inter)
”	”	”	”	160	GPS	*Metois et al.* (2016)	No (co>inter)
”	”	”	”	116	EQ	*Lay et al.* (2014)	Yes (co>inter)
Chile 2	-23.12/-71.26	68	72	156	GPS	*Chlieh et al.* (2011)	No (contrad.)
”	”	”	”	133	GPS	*Metois et al.* (2016)	No (contrad.)
”	”	”	”	70	GPS	*Saillard et al.* (2017)	No (contrad.)
”	”	”	”	71	GPS	*Béjar-Pizarro et al.* (2013)	No (contrad.)
Chile 3	-26.34/-71.62	81	98	96	GPS	*Metois et al.* (2013)	No (contrad.)
”	”	”	”	172	GPS	*Metois et al.* (2016)	No (contrad.)
”	”	”	”	123	GPS	*Saillard et al.* (2017)	No (contrad.)
”	”	”	”	113	GPS	*Metois et al.* (2012)	No (contrad.)
Chile 4	-31.14/-72.59	85	89	93	GPS	*Metois et al.* (2013)	No (co>inter)
”	”	”	”	113	GPS	*Metois et al.* (2016)	No (co>inter)
”	”	”	”	101	GPS	*Saillard et al.* (2017)	No (co>inter)
”	”	”	”	95	GPS	*Metois et al.* (2012)	No (co>inter)
”	”	”	”	84	EQ	*Yue et al.* (2014)	Yes (co>inter)
Chile 5	-34.48/-73.50	119	134	140	GPS	*Metois et al.* (2012)	No (co>inter)
”	”	”	”	181	GPS	*Saillard et al.* (2017)	No (co>inter)
”	”	”	”	144	GPS	*Metois et al.* (2016)	No (co>inter)
”	”	”	”	113	EQ	*Li et al.* (2016)	Yes (co>inter)

References

Béjar-Pizarro, M., A. Socquet, R. Armijo, D. Carrizo, J. Genrich, and M. Simons (2013), Andean structural control on interseismic coupling in the North Chile subduction zone, *Nature Geoscience*, *6*(6), 462–467.

Briggs, R. W., K. Sieh, A. J. Meltzner, D. Natawidjaja, J. Galetzka, B. W. Suwargadi, Y. J. Hsu, M. Simons, N. Hananto, I. Suprihanto, D. Prayudi, J.-P. Avouac, L. Prawirodirdjo, and Y. Bock (2006), Deformation and slip along the Sunda Megathrust in the great 2005 Nias-Simeulue earthquake, *Science*, *311*(5769), 1897–1901.

Burgette, R. J., R. J. Weldon II, and D. A. Schmidt (2009), Interseismic uplift rates for western Oregon and along-strike variation in locking on the Cascadia subduction zone, *Journal of Geophysical Research*, *114*(B1), TC3009–24.

Bürgmann, R. (2005), Interseismic coupling and asperity distribution along the Kamchatka subduction zone, *Journal of Geophysical Research*, *110*(B7), 1675–17.

Chlieh, M., J.-P. Avouac, K. Sieh, D. H. Natawidjaja, and J. Galetzka (2008), Heterogeneous coupling of the Sumatran megathrust constrained by geodetic and paleogeodetic measurements, *Journal of Geophysical Research*, *113*(B5), 2018–31.

Chlieh, M., H. Perfettini, H. Tavera, J.-P. Avouac, D. Remy, J.-M. Nocquet, F. Rolandone, F. Bondoux, G. Gabalda, and S. Bonvalot (2011), Interseismic coupling and seismic potential along the Central Andes subduction zone, *Journal of Geophysical Research*, *116*(B12), B10,404–21.

Cross, R. S., and J. T. Freymueller (2007), Plate coupling variation and block translation in the Andreanof segment of the Aleutian arc determined by subduction zone modeling using GPS data, *Geophysical Research Letters*, *34*(6), 1653–5.

Edwards, J. H., J. W. Kluesner, E. A. Silver, and N. L. Bangs (2018), Pleistocene vertical motions of the Costa Rican outer forearc from subducting topography and a migrating fracture zone triple junction, *Geosphere*, pp. 1–25.

Franco, A., C. Lasserre, H. Lyon-Caen, V. Kostoglodov, E. Molina, M. Guzman-Speziale, D. Monterosso, V. Robles, C. Figueroa, W. Amaya, E. Barrier, L. Chiquin, S. Moran, O. Flores, J. Romero, J. A. Santiago, M. Manea, and V. C. Manea (2012), Fault kinematics in northern Central America and coupling along the subduction interface of the Cocos Plate, from GPS data in Chiapas (Mexico), Guatemala and El Salvador, *Geophysical Journal International*, *189*(3), 1223–1236.

Hashimoto, C., A. Noda, T. Sagiya, and M. Matsu'ura (2009), Interplate seismogenic zones along the Kuril-Japan trench inferred from GPS data inversion, *Nature Geoscience*, *2*(2), 141–144.

Hyndman, R. D., K. Wang, and M. Yamano (1995), Thermal constraints on the seismogenic portion of the southwestern Japan subduction thrust, *Journal of Geophysical Research: Planets*, *100*(B8), 15,373–15,392.

Johnson, J. M. (1998), Heterogeneous Coupling Along Alaska-Aleutians as Inferred From Tsunami, Seismic, and Geodetic Inversions, in *Tsunamigenic Earthquakes and Their Consequences*, pp. 1–116, Elsevier.

Johnson, J. M., Y. Tanioka, L. J. Ruff, K. Satake, H. Kanamori, and L. R. Sykes (1994), The 1957 great Aleutian earthquake Pure Applied Geophysics, 142 (1), 1994, pp 3–28, *Pure and Applied Geophysics*, *142*(1), 3–28.

Kanamori, H., and K. C. McNally (1982), Variable rupture mode of the subduction zone along the Ecuador-Colombia coast, *Bulletin of the Seismological Society of America*, *72*(4), 1241–1253.

LaFemina, P., T. H. Dixon, R. Govers, E. Norabuena, H. Turner, A. Saballos, G. Mattioli, M. Protti, and W. Strauch (2009), Fore-arc motion and Cocos Ridge collision in Central America, *Geochemistry Geophysics Geosystems*, *10*(5), n/a–n/a.

Lay, T., C. J. Ammon, H. Kanamori, L. Xue, and M. J. Kim (2011), Possible large near-trench slip during the 2011 $M_w 9.0$ off the Pacific coast of Tohoku Earthquake, *Earth, Planets and Space*, *63*(7), 687–692.

Lay, T., H. Kanamori, C. J. Ammon, K. D. Koper, A. R. Hutko, L. Ye, H. Yue, and T. M. Rushing (2012), Depth-varying rupture properties of subduction zone megathrust faults, *Journal of Geophysical Research*, *117*(B4), n/a–n/a.

Lay, T., H. Yue, E. E. Brodsky, and C. An (2014), The 1 April 2014 Iquique, Chile, $M_w 8.1$ earthquake rupture sequence, *Geophysical Research Letters*, *41*(11), 3818–3825.

Li, L., T. Lay, K. F. Cheung, and L. Ye (2016), Joint modeling of teleseismic and tsunami wave observations to constrain the 16 September 2015 Illapel, Chile, $M_w 8.3$ earthquake rupture process, *Geophysical Research Letters*, *43*(9), 4303–4312.

Loveless, J. P., and B. J. Meade (2010), Geodetic imaging of plate motions, slip rates, and partitioning of deformation in Japan, *Journal of Geophysical Research*, *115*(B2), L11,303–35.

McCaffrey, R., A. I. Qamar, R. W. King, R. Wells, G. Khazaradze, C. A. Williams, C. W. Stevens, J. J. Vollick, and P. C. Zwick (2007), Fault locking, block rotation and crustal deformation in the Pacific Northwest, *Geophysical Journal International*, *169*(3), 1315–1340.

Metois, M., A. Socquet, and C. Vigny (2012), Interseismic coupling, segmentation and mechanical behavior of the central Chile subduction zone, *Journal of Geophysical Research*, *117*(B3), 40–16.

Metois, M., C. Vigny, A. Socquet, A. Delorme, S. Morvan, I. Ortega, and C. M. Valderas-Bermejo (2013), GPS-derived interseismic coupling on the subduction and seismic hazards in the Atacama region, Chile, *Geophysical Journal International*, *196*(2), 644–655.

Metois, M., C. Vigny, and A. Socquet (2016), Interseismic Coupling, Megathrust Earthquakes and Seismic Swarms Along the Chilean Subduction Zone (38°–18°S), *Pure and Applied Geophysics*, *173*(5), 1431–1449.

Natawidjaja, D. H., K. Sieh, J. Galetzka, B. W. Suwargadi, H. Cheng, R. L. Edwards, and M. Chlieh (2007), Interseismic deformation above the Sunda Megathrust recorded in coral microatolls of the Mentawai islands, West Sumatra, *Journal of Geophysical Research-Solid Earth and Planets*, *112*(B2), 1897–27.

Nocquet, J.-M., J. C. Villegas-Lanza, M. Chlieh, P. A. Mothes, F. Rolandone, P. Jarrin, D. Cisneros, A. Alvarado, L. Audin, F. Bondoux, X. Martin, Y. Font, M. Régnier, M. Vallée, T. Tran, C. Beauval, J. M. Maguiña Mendoza, W. Martinez, H. Tavera, and H. Yepes (2014), Motion of continental slivers and creeping subduction in the northern Andes, *Nature Geoscience*, *7*(4), 287–291.

Park, J.-O., T. Tsuru, S. Kodaira, P. R. Cummins, and Y. Kaneda (2002), Splay Fault Branching Along the Nankai Subduction Zone, *Science*, *297*(5584), 1157–1160.

Radiguet, M., F. Cotton, M. Vergnolle, M. Campillo, A. Walpersdorf, N. Cotte, and V. Kostoglodov (2012), Slow slip events and strain accumulation in the Guerrero gap, Mexico, *Journal of Geophysical Research*, *117*(B4), n/a–n/a.

Saillard, M., L. Audin, B. Rousset, J.-P. Avouac, M. Chlieh, S. R. Hall, L. Husson, and D. L. Farber (2017), From the seismic cycle to long-term deformation: linking seismic coupling and Quaternary coastal geomorphology along the Andean megathrust, *Tectonics*, *36*(2), 241–256.

Schmalzle, G. M., R. McCaffrey, and K. C. Creager (2014), Central Cascadia subduction zone creep, *Geochemistry Geophysics Geosystems*, *15*(4), 1515–1532.

Stock, J. M., and J. Lee (2010), Do microplates in subduction zones leave a geological record?, *Tectonics*, *13*(6), 1472–1487.

Sykes, L. R., J. B. Kisslinger, L. House, J. N. Davies, and K. H. Jacob (1981), Rupture Zones and Repeat Times of Great Earthquakes Along the Alaska-Aleutian ARC, 1784–1980, in *Earthquake Prediction An International Review*, edited by D. W. Simpson and P. G. Richards, pp. 73–80, American Geophysical Union, Washington, D. C.

Wallace, L. M. (2004), Subduction zone coupling and tectonic block rotations in the North Island, New Zealand, *Journal of Geophysical Research*, *109*(B12), 477–21.

Wang, K., and A. M. Tréhu (2016), Invited review paper: Some outstanding issues in the study of great megathrust earthquakes—The Cascadia example, *Journal of Geodynamics*, *98*, 1–18.

Wang, K., R. Wells, S. Mazzotti, R. D. Hyndman, and T. Sagiya (2003), A revised dislocation model of interseismic deformation of the Cascadia subduction zone, *Journal of Geophysical Research*, *108*(B1), 1085–13.

Ye, L., T. Lay, and H. Kanamori (2013), Large earthquake rupture process variations on the Middle America megathrust, *Earth and Planetary Science Letters*, *381*(C), 147–155.

Yue, H., T. Lay, L. Rivera, C. An, C. Vigny, X. Tong, and J. C. Báez Soto (2014), Localized fault slip to the trench in the 2010 Maule, Chile $M_w = 8.8$ earthquake from joint inversion of high-rate GPS, teleseismic body waves, InSAR, campaign GPS, and tsunami observations, *Journal of Geophysical Research*, *119*(10), 7786–7804.